ADVANCED ENERGY MATERIALS
www.advenergymat.de

Considering the Role of Ion Transport in Diffuson-Dominated Thermal Conductivity

Tim Bernges, Riley Hanus, Bjoern Wankmiller, Kazuki Imasato, Siqi Lin, Michael Ghidiu, Marius Gerlitz, Martin Peterlechner, Samuel Graham, Geoffroy Hautier, Yanzhong Pei, Michael Ryan Hansen, Gerhard Wilde, G. Jeffrey Snyder, Janine George, Matthias T. Agne, and Wolfgang G. Zeier**

Next-generation thermal management requires the development of low lattice thermal conductivity materials, as observed in ionic conductors. For example, thermoelectric efficiency is increased when thermal conductivity is decreased. Detrimentally, high ionic conductivity leads to thermoelectric device degradation. Battery safety and design also require an understanding of thermal transport in ionic conductors. Ion mobility, structural complexity, and anharmonicity have been used to explain the thermal transport properties of ionic conductors. However, thermal and ionic transport are rarely discussed in direct comparison. Herein, the ionic conductivity of Ag^+ argyrodites is found to change by orders of magnitude without altering the thermal conductivity. Thermal conductivity measurements and two-channel lattice dynamics modeling reveal that the majority of Ag^+ vibrations have a non-propagating diffuson-like character, similar to amorphous materials. It is found that high ionic mobility is not a requirement for diffuson-mediated transport. Instead, the same bonding and structural traits that can lead to fast ionic conduction also lead to diffuson-mediated transport. Bridging the fields of solid-state ionics and thermal transport, it is proposed that a vibrational perspective can lead to new design strategies for functional ionic conducting materials. As a first step, the authors relate the so-called Meyer–Neldel behavior in ionic conductors to phonon occupations.

1. Introduction

Low lattice thermal conductivities (κ_L), as often found in fast ionic conductors, are greatly beneficial for thermoelectric devices where the thermoelectric efficiency metric zT scales inversely with κ_L, following $zT = S^2\sigma T/(\kappa_L + \kappa_e)$. A prominent idea to explain the low thermal conductivity values found in ionic conductors is based on the "Phonon Liquid Electron Crystal (PLEC)" concept.[1–5] Taken literally, the PLEC concept describes the conducting ionic species to behave liquid-like within a rigid structural matrix. Some propose that this ultimately causes a reduction of the specific heat capacity.[1,3] The caveat is that the magnitude and temperature-dependence of ionic conduction are not typically reported,[6] so it is not clear how "liquid-like" these materials really are, nor is it clear if the occurrence of ionic transport is fundamentally responsible for the observed low thermal conductivity values

T. Bernges, B. Wankmiller, M. Ghidiu, W. G. Zeier
Institute of Inorganic and Analytical Chemistry
University of Münster
D-48149 Münster, Germany
E-mail: wzeier@uni-muenster.de

R. Hanus, S. Graham
George W. Woodruff School of Mechanical Engineering
Georgia Institute of Technology
Atlanta, GA 30332, USA

B. Wankmiller, M. R. Hansen
Institute of Physical Chemistry
University of Münster
D-48149 Münster, Germany

The ORCID identification number(s) for the author(s) of this article can be found under https://doi.org/10.1002/aenm.202200717.

DOI: 10.1002/aenm.202200717

B. Wankmiller
International Graduate School for Battery Chemistry
Characterization
Analysis
Recycling and Application (BACCARA)
University of Münster
D-48149 Münster, Germany

K. Imasato
Global Zero Emission Research Center
National Institute of Advanced Industrial Science and Technology (AIST)
Tsukuba, Ibaraki 305-8569, Japan

S. Lin, Y. Pei
Interdisciplinary Materials Research Center
School of Materials Science and Engineering
Tongji University
Shanghai 201804, China

M. Gerlitz, M. Peterlechner, G. Wilde
Institute of Materials Physics
University of Münster
D-48149 Münster, Germany

G. Hautier
Institute of Condensed Matter and Nanoscience
Université Catholique de Louvain
1348 Ottignies-Louvain-la-Neuve, Belgium

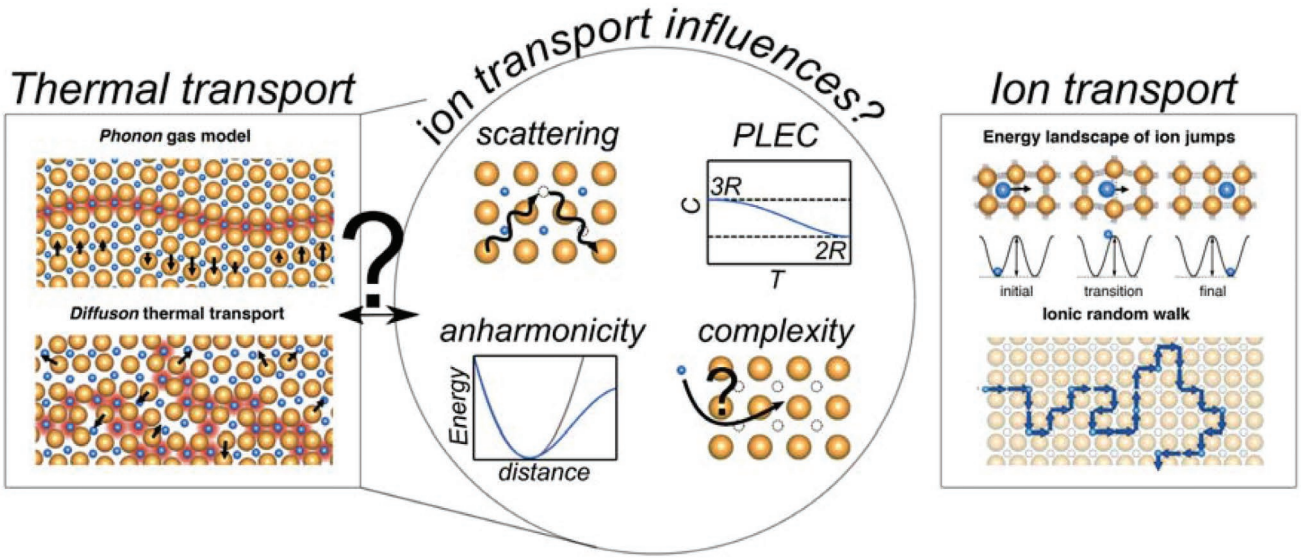

Figure 1. Schematic representation of thermal transport, ionic transport, and their possible interactions. (left) A long-range phonon mode with correlated atomic displacements (black arrows) carries heat (in red) analogous to a gas (phonon gas model, top). Diffusons (bottom), with a low correlation of atomic displacements (black arrows), transfer heat (in red) on a local scale as a random walk. (middle) Possible ion transport influences on thermal transport include the scattering of propagating modes by structural disorder (e.g., point-defects) and anharmonicity (phonon-phonon scattering), a reduction in heat capacity according to the "Phonon Liquid Electron Crystal (PLEC)" concept and increased structural complexity leading to a large number of phonon branches. (right) Schematic of an ion jump event and corresponding energy landscape (top) and ion transport depicted as a random walk (portion of random walk shown, bottom).

in these materials. In fact, it has been recently shown that at least some fast ionic conductors still exhibit crystalline phonon properties despite their mobile ion sublattice.[4,5]

The influence of ionic motion on thermal transport has been discussed in the context of classic phonon-gas transport, where heat transport by phonons is thought to occur in a propagating manner on a length-scale much larger than interatomic distances (phonon-gas model, **Figure 1**, left).[7,8] Here, it is suggested that the scattering of propagating phonon quasiparticles can be increased by (static and dynamic) point-defects, the inherent anharmonicity associated with ionic jumps,[4,9] and the increased configurational complexity of the material, e.g., the atomic arrangement and distribution throughout the lattice (shown schematically in Figure 1).[4,5,10,11] This phonon-gas like thermal transport is commonly observed in structurally simple and crystalline thermoelectric materials like PbTe.[12]

A fundamentally different heat transport mechanism, i.e., a second type of phonon transport, is via the diffuson.[13,14] In contrast to propagating phonons (phonon-gas model), diffusons carry heat via local scale random walk facilitated by coupling of vibrational modes.[15,16] This diffusive heat transport[17] means that non-propagating (but extended) vibrations in a solid transfer thermal energy between adjacent diffuson modes,[14,15] at a much smaller length scale compared to typical propagating modes (shown schematically in Figure 1 left). Diffusons are enabled and facilitated by a large number of phonon branches in close energetic proximity due to structural complexity and by anharmonicity (contributing to quasi degeneracy).[16] While diffuson-mediated transport was first observed and described in amorphous materials,[13,18] recently it was shown that significant diffuson contributions exist in complex crystalline thermoelectric materials, e.g., $Yb_{14}MnSb_{11}$.[16]

Fast ion transport has also been associated with diffuson-like signatures in inelastic neutron scattering experiments and ab initio molecular dynamics calculations.[4,9] As complexity, anharmonicity, and fast ion transport, are commonly found in both state-of-the-art solid electrolytes for battery applications, e.g., Na_3PS_4 and Li_6PS_5Cl,[19–21] and promising thermoelectric materials such as Ag_9GaSe_6, Cu_2Se and (Ag,Cu)$CrSe_2$,[1,4,5,10,20,22–24] there is an outstanding question if diffusons play a significant role in their thermal conductivity. In fact, many Ag^+ and Cu^+ conducting argyrodites have thermal conductivities below the theoretical "minimum" thermal conductivity proposed for purely propagating transport,[10,11,25,26] which may be explained

G. Hautier
Dartmouth College
Thayer School of Engineering
Hanover, NH 03755, USA
G. J. Snyder
Department of Materials Science and Engineering
Northwestern University
Evanston, IL 60208, USA
J. George
Federal Institute for Materials Research and Testing (BAM)
D-12205 Berlin, Germany
J. George
Institute of Condensed Matter
Theory and Solid-State Optics
Friedrich Schiller University
07743 Jena, Germany
M. T. Agne, W. G. Zeier
Institut für Energie- und Klimaforschung (IEK)
IEK-12: Helmholtz-Institut Münster
Forschungszentrum Jülich
48149 Münster, Germany
E-mail: m.agne@fz-juelich.de

by diffuson-mediated transport. Furthermore, Cheng et al. recently reported "glass-like" thermal transport behavior of different Li^+ and Na^+ solid electrolyte classes, which is consistent with diffuson transport.[20]

Generally, there are strong underlying physical similarities between thermal diffusons and ionic diffusion: 1) fast ionic transport is achieved in strongly disordered materials[22,24] and strong disorder promotes the prevalence of thermal transport via diffusons.[15] 2) Both transport phenomena operate within an atomic-scale random walk, in which local vibrations carry and transfer thermal energy or momentum of ions (Figure 1).[15,27] 3) Anharmonic lattice vibrations enhance diffuson-mediated transport[17] and, although the characteristic vibration of a mobile ion is usually shown using a harmonic potential well, an ion jump is an intrinsically anharmonic process.[28]

On a fundamental level, thermal transport arises from fluctuations of the phonon occupation number,[29–31] i.e., the thermodynamic drive to have a constant phonon occupation (thermal energy) throughout the entire material. Here, the phonon occupation number describes the excitation state (energy level) of the vibrational mode in the harmonic oscillator definition of phonons.[29] While not commonly discussed in terms of phonon occupation numbers, ionic transport can be thought of as a thermal fluctuation (phonon occupation number fluctuation) that is energetically capable of moving the ion across a barrier between adjacent lattice sites.[27] The magnitude of the fluctuation needed to move an ion is significantly increased, relative to thermal transport, since the ion has to surpass this activation barrier.[23] Despite their differences, both transport processes can thus be related on a microscopic scale using phonon occupations. Nevertheless, without quantitative measures of ionic transport, it is not possible to ascertain its role in thermal conductivity.

Here, the thermal and ionic transport, as well as the vibrational properties, of nine Ag^+ argyrodite compositions are investigated, some of which are promising high-efficiency thermoelectric materials.[25,34–36] This work aims to decouple the influences of ionic transport, structural complexity, and anharmonicity on the vibrational character and corresponding thermal conductivity of these fast ion conductors. By experimentally quantifying ionic conductivity and thermal conductivity, in conjunction with state-of-the-art computational methods, we are able to address the following questions: 1) Are significant diffuson contributions to thermal conductivity present in the here investigated fast ionic conductors? 2) Which vibrational modes characterize both transport processes and 3) is the character of these vibrational modes and their transport of thermal energy altered by changing ionic transport by orders of magnitude?

Especially question 3 is of significant relevance. High ionic conductivities hinder the long-term stability of superionic conductors in thermoelectric devices[37] and batteries, comprised of ionic conductors, need thermal management to decrease charging times and improve safety.[38] In addition, the discussion of ionic transport from a viewpoint of phonon occupation fluctuations leads to a new interpretation of so-called Meyer–Neldel behavior. Understanding this interrelation of the migration enthalpy and entropy is paramount for the design of faster solid ionic conductors.[23,32,39]

2. Results and Discussion

To answer these questions, a successful isovalent substitution from Ag_8SiSe_6 to Ag_8GeSe_6 and Ag_8SnSe_6 is achieved as shown by the linear increase of the lattice volume determined from Rietveld refinements of X-ray diffraction measurements (Note S1 and S2, Supporting Information).[40] These materials are fast ionic conductors and have been intensely investigated for their thermoelectric transport properties due to their low thermal conductivity.[10,25,41] The different compositions have varying room-temperature structures,[35,42] but ultimately undergo a phase transition into the same cubic structure that is characterized by its strongly disordered Ag^+ sublattice at high temperatures (Note S2, Supporting Information).[10,25] Structurally, there are a large number of Ag^+ sites that are tetrahedrally coordinated and have face-sharing connectivity. These sites have an average occupation of only 25 %. While the low-temperature phase of Ag_8SiSe_6 is cubic with an ordered Ag^+ sublattice,[35] both Ag_8GeSe_6 and Ag_8SnSe_6 crystallize in an orthorhombic structure at room-temperature (Note S2, Supporting Information). In the orthorhombic phase, the Ag^+ sublattice consists of five distinct and fully occupied lattice sites, each either tetrahedrally or trigonally coordinated by Se^{2-} arranged in a corner- or edge-sharing fashion, respectively.

Expanding the structural analysis over a broad temperature range additionally allows determining the phase transition temperatures (Note S2, Supporting Information) and assessing the thermal expansion behavior. The latter was not significantly altered upon substitution, with thermal expansion coefficients ranging from 7.7 to 8.7×10^{-5} K^{-1}, with an average of $8.2 \pm 0.5 \times 10^{-5}$ K^{-1} for all compositions. Furthermore, the temperature dependent analysis was utilized to extract information about the dynamics of the Ag^+ sublattice by tracking their thermal displacements, which will be discussed later.

While compositional changes to the local and average structure of a material are known to play a significant role in the ionic and thermal transport behavior,[7,23] they do not seem to have a strong effect on the primary conclusions of this work. Therefore, we focus on characterizing the thermal and ionic transport in context of the vibrational properties. This characterization allows us to directly compare and ascertain the role of ionic transport on thermal conductivity, both macroscopically and microscopically.

2.1. Diffuson-Mediated Thermal Transport

The low thermal conductivities of fast ionic conductors are often attributed to (static and dynamic) atomic disorder, anharmonicity and complex crystal structure, in addition to overall soft bonding and low-frequency optical phonon modes.[11] All of these parameters are commonly associated with either lowering the phonon group-velocity or increasing the phonon scattering rate, in context of the phonon-gas model.[10,25,41] While these structural and vibrational features are likely to factor into the characteristics of thermal transport, the vicinity to the Ioffe-Regel limit and the associated concept of a minimum lattice thermal conductivity[13,15,43] suggests that the phonon-gas model is possibly an incomplete description of thermal transport in

these systems. Here, the Ioffe-Regel limit refers to the condition when propagating modes are scattered so frequently that the gas-like description of phonons breaks down, i.e., the wavevector is no longer well-defined.[43] Instead, thermal energy can be transferred by wave-like tunneling,[17] which has been described as a random walk.[15] These non-propagating phonons, called diffusons, are expected to play a significant role in thermal transport in vicinity of the Ioffe-Regel limit.[14]

The measured high-temperature lattice thermal conductivities (**Figure 2**a, Note S3, Supporting Information) show a flat temperature dependence typical for diffuson-mediated transport with values in the range from 0.15 W m^{-1} K^{-1} to 0.32 W m^{-1} K^{-1} (at 475 K) for the varying compositions. Given the experimental uncertainty, here determined to be ± 0.05 W m^{-1} K^{-1} (shown in Figure 2a) from the measurement of three samples of Ag_8GeSe_6, and the lack of a clear compositional dependence (Note S3, Supporting Information), the thermal conductivities are better described by an average value of 0.21 ± 0.05 W m^{-1} K^{-1} (again at 475 K). Therefore, no significant changes in thermal transport with composition are observed here, which is later rationalized by our spectral and vibrational analysis. Our uncertainty estimation is also in accordance with the relatively large spread of reported lattice thermal conductivities of the Ag^+ argyrodites.[44–46]

All measured lattice thermal conductivities are consistently below the theoretical "minimum" thermal conductivity expected from a phonon-gas model and in good alignment with the estimations of a diffuson model (Figure 2a, Note S4, Supporting Information).[15,43] Here, the limits are calculated according to Cahill et al.[43] (phonon-gas limit) and Agne et al.[15] (diffuson limit) utilizing the measured speeds of sound (Note S4, Supporting Information) and the shadings represent the regimes above the phonon-gas limit (orange, Figure 2a) and below the diffuson limit (green, Figure 2a). These models consider what thermal conductivity can be expected when all vibrational modes behave purely phonon-gas-like or diffuson-like,

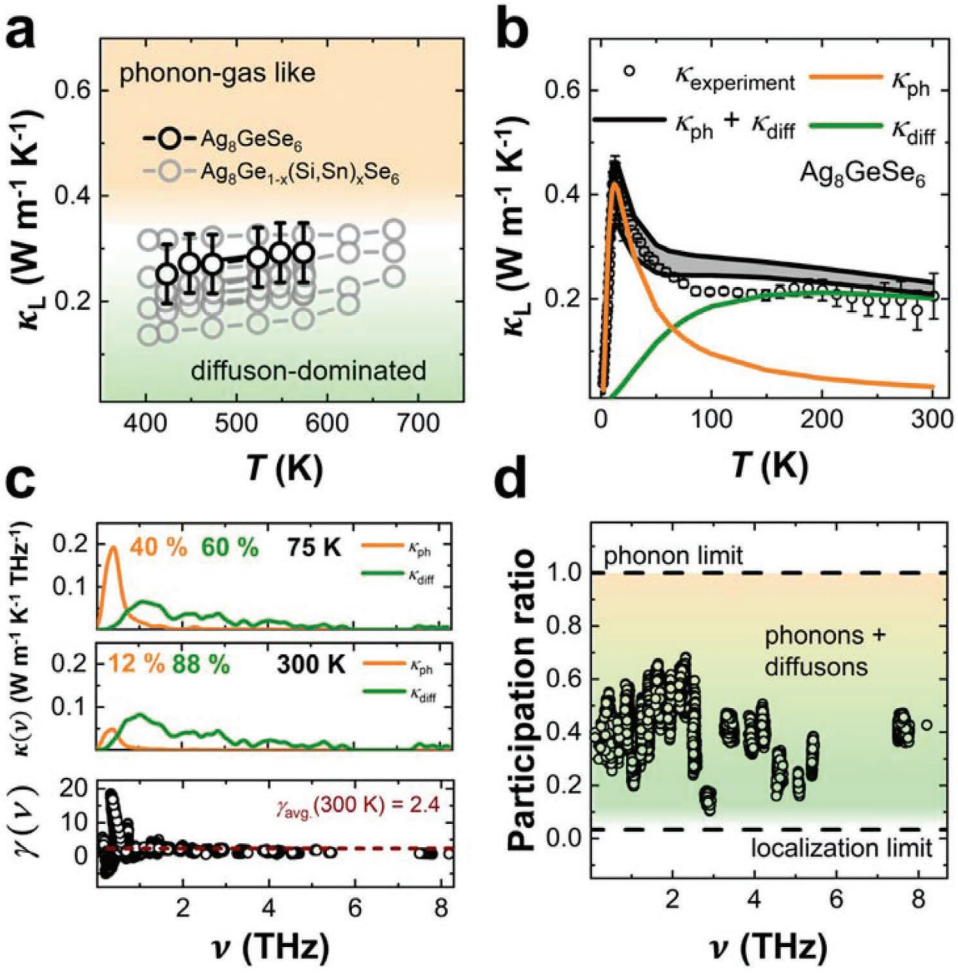

Figure 2. Vibrational character and thermal transport in Ag_8GeSe_6. a) The high-temperature lattice thermal conductivity of Ag_8GeSe_6 and all other compositions (in grey) in comparison to the theoretical phonon-gas-dominated (above the Cahill limit, orange shading) and diffuson-dominated (below the diffuson limit, green shading) regimes. b) Experimental lattice thermal conductivity measurements from 2 to 300 K, and the corresponding two-channel lattice dynamical transport model, indicate a transition from phonon-gas-like (below 100 K) to diffuson-dominated thermal transport (above 100 K). c) The spectral phonon-gas and diffuson-like thermal conductivity at 75 and 300 K and the spectral Grüneisen parameter. d) The participation ratios of the vibrational modes are well below the phonon limit for spatially extended modes (dashed line, participation-ratio = 1) and comparable to amorphous materials.[26]

respectively.[15] Despite the simplicity of this assessment, it gives the first indication of diffuson contributions to thermal transport.

To confirm the hypothesis of diffuson-like thermal transport at high temperature, low-temperature thermal conductivities were measured. Here, the lattice thermal conductivity of Ag_8GeSe_6 shows that the flat-temperature dependence persists down to 100 K before a phonon peak arises around 12 K, with a thermal conductivity of just ≈ 0.5 W m^{-1} K^{-1} (Figure 2b). This temperature dependence was confirmed by corresponding low-temperature measurements of the other end members Ag_8SiSe_6 and Ag_8SnSe_6 (see Note S3, Supporting Information).

Two-channel modeling based on the calculated lattice dynamics for the orthorhombic phase of Ag_8GeSe_6 is utilized to explain these results (details in Notes S5 and S6, Supporting Information). Here, the heat current operator matrix is analyzed regarding its diagonal (phonon-gas-like) and off-diagonal (diffuson-like) elements such that the total lattice thermal conductivity of the two-channel model is $\kappa_L = \kappa_{ph} + \kappa_{diff}$.[16] Adding the conductivities in parallel ensures that the total number of vibrations (heat capacity) remains constant, but acknowledges that the vibrations can interact with each other in fundamentally different ways.[16] Given the computational cost of third and fourth order force constants, an analytical scattering model was implemented to describe the temperature dependence of the phonon lifetimes (details in Note S6, Supporting Information).[16] The analytical model considers phonon-phonon scattering (τ_p^{-1}) and boundary scattering (τ_b^{-1}) resulting in a total scattering rate of

$$\tau^{-1} = \tau_p^{-1} + \tau_b^{-1} = C_1\omega^2 T \cdot e^{-\frac{C_2}{T}} + A\omega \quad (1)$$

with C_1, C_2 and A as constants that describe the experimental data. The constant C_1 captures Umklapp processes and generally depends on the materials density, stiffness of the lattice, and anharmonicity, while A describes boundary scattering and is dependent on the microstructure of the sample (e.g., the grain size).[8,47] The additional temperature dependence of the phonon-phonon scattering term C_2, captures the transition from Normal to Umklapp processes.[8,29] It is important to recognize that Equation (1) is used to describe all of the vibrational modes, and thus captures both phonon-gas- and diffuson-like transport when the interaction between vibrational modes is considered (Note S6, Supporting Information).

Given the excellent agreement of the two-channel model with the experimental results (Figure 2b), Equation (1) captures the essential phonon physics of this material well. Nevertheless, it should be emphasized that the main conclusions are insensitive to the choice of the analytical scattering function. Corresponding results utilizing a simplified phonon-phonon scattering term are shown in the Supporting Information, confirming the predominance of diffuson contributions to thermal transport at high temperatures (Note S6, Supporting Information).

The resulting phonon gas channel contributions, κ_{ph}, dominate the total lattice thermal conductivity at low temperatures and well-describe the peak in thermal conductivity (Figure 2b). With increasing temperature, the phonon-gas channel declines while vice versa the diffuson contributions, κ_{diff}, increase strongly, before plateauing above 100 K. The reason that the high temperature contributions of κ_{ph} are much lower than the Cahill phonon-gas limit (Figure 2a) is because only ≈ 15% of phonons conduct heat in a propagating manner (as shown later by our spectral analysis, Figure 2c), while the Cahill model assumes that all vibrations behave phonon-gas like. The resulting total lattice thermal conductivity of the two-channel model, $\kappa_L = \kappa_{ph} + \kappa_{diff}$, captures both the magnitude and temperature-dependence of the experimental data, not only in the phonon-gas ($T < 50$ K) and diffuson ($T > 100$ K) mediated regimes but also at temperatures where both channels have similar contributions. The two lines shown for the total calculated lattice thermal conductivity (bounded-grey region in Figure 2b) represent the upper- and lower-limit of the calculation, stemming from a slight anisotropy of the orthorhombic structure (for details see Note S6, Supporting Information). The thermal conductivity of single-crystal Ag_8SnSe_6 was found to have a similar anisotropy at 300 K.[48]

The two-channel model additionally allows for a spectral analysis of the thermal conductivity of both channels (Figure 2c, top). The contributions from the phonon gas channel arise from the lowest frequency modes below 1 THz (≈ 15% of the phonons), while the spectral thermal conductivity of the diffuson channel is extended over the whole frequency range. A close-up of the low and intermediate frequency regime can be found in Note S6, Supporting Information. Note that the spectral thermal conductivity is not expected to be zero at zero frequency but it is an artifact commonly seen when uniform q-meshing is used and is associated with poor Brillouin zone sampling near the Gamma point.[8] While this influences the spectral decompositions, it typically has little impact on integrated thermal conductivity values. Nevertheless, the spectral analysis leads to the important conclusion that phonons at temperatures relevant for ion transport have a predominantly diffuson-like character (88% diffusons at 300 K) and that high-frequency vibrations (>4 THz, Figure 2c) marginally contribute to thermal transport. These high-frequency modes are related to the here-substituted species (Ge, Sn and Si, Note S5, Supporting Information), which explains our observation that thermal transport is not significantly altered upon changes to the composition (Figure 2a).

Evaluation of the mode-specific Grüneisen parameters (Figure 2c, bottom, Note S5, Supporting Information), which indicate the anharmonicity of each phonon mode, lends an explanation for the strong decline of the phonon gas channel with temperature. Here, large Grüneisen parameters are found in the same frequency range in which the phonon-gas channel contributions are the strongest (Figure 2c, top, Note S6, Supporting Information). Meanwhile, the average calculated Grüneisen parameter at 300 K is 2.4 and with that close to the compositional average of 1.9 ± 0.3 obtained from speed of sound measurements[49] (Note S4, Supporting Information). Therefore, the extensive anharmonicity, especially at low frequencies, is believed to be the driving factor for the strong suppression of the phonon-gas channel and the subsequent transition to diffuson-dominated thermal transport. The large Umklapp scattering rates associated with such extensive anharmonicities were captured phenomenologically by our analytical

scattering function (Equation 1). It is not surprising that such large Grüneisen parameters exist since anharmonic vibrations have been linked to ion conducting materials.[4,5,9,50]

Having assessed the vibrational character of phonon modes, i.e., phonon-gas- or diffuson-like, from thermal transport behavior, it is also possible to characterize the vibrational character directly from the mode eigenvectors. In addition to having a frequency, each phonon mode has an eigenvector that defines the vibration direction of each atom in the material as well as the relative participation of each atom in the phonon mode.[29,31] The spatial extension and "shape" of phonon modes have been used previously to distinguish vibrational characters.[13,31,51] Here, we use the participation ratio for such analysis (Figure 2d, details in Note S7, Supporting Information).[13,31] A participation ratio close to unity is indicative of a high spatial extension of a mode and typically found in simple crystalline materials like c-Si that have textbook phonon-gas transport,[13] and so a participation ratio of 1 can be called the phonon limit. Participation ratios below ≈0.1 are typical for localized modes that do not contribute to thermal transport, and the localization limit is, by definition, when only 1 atom (out of all the atoms in the unit cell) participates in the vibrational mode.[31] The calculated participation ratios are in the intermediate range, comparable to those of amorphous materials like a-C and a-SiO_2,[31] despite the crystalline and ordered nature of the low-temperature orthorhombic Ag_8GeSe_6 phase. While the participation ratio cannot clearly separate phonons and diffusons,[31,51] the similarity to the results of amorphous materials strongly indicates the presence of diffuson-like vibrations complementary to the two-channel model. Additionally, the participation ratio analysis reveals that fully-localized modes (locons) do not play an important role in the argyrodites.

These results validate our initial hypothesis of diffuson-mediated thermal transport in the Ag^+ argyrodite Ag_8GeSe_6 at temperatures relevant for thermoelectrics and ionic conduction. While the corresponding high-temperature results for all compositions and low-temperature results for Ag_8SiSe_6 and Ag_8SnSe_6 (Note S3, Supporting Information) strongly indicate that diffuson-dominated transport can be generalized to all compositions, it has yet to be shown that the vibrational properties are not significantly altered by substitution. To do so, the vibrational range of the Ag^+ modes is assessed experimentally utilizing Einstein frequencies (as obtained from temperature dependent X-ray diffraction), while the average vibrational properties are tracked by Debye frequencies (determined from speed of sound measurements) for all compositions. This analysis will reveal that the main contribution to diffuson-transport originates from vibrations of the Ag^+ ions.

2.2. Vibrational Frequencies

The vibrational spectrum of a material has significant importance for the fields of thermal and ionic conduction.[8,23,39,52] Commonly, the Debye frequency ν_D is used to approximate the dynamics of the material and estimate the thermal conductivity of a material based on the phonon-gas or diffuson model (Note S4, Supporting Information).[7,15] However, in disordered and soft materials, the Debye-frequency often fails its original purpose to estimate the maximum vibrational frequency, but rather falls into the center of the vibrational density of states.[15,19] With that, it provides a useful experimental insight into the average dynamics of the lattice.[19] When considering ionic transport, the attempt frequency of the mobile species is included explicitly in the Arrhenius prefactor (Note S8, Supporting Information).[21,23] While the Debye frequency is frequently used to approximate the attempt frequency, it does not directly refer to vibrations of the mobile ion. Here, a better experimental descriptor for the attempt frequency would be a vibrational frequency ν_E specific for the mobile ion that is conceptually similar to an Einstein oscillator.[53,54]

We assess the experimental average Ag^+ vibrational frequency by measuring the isotropic thermal displacement of Ag^+ ions using temperature dependent X-ray diffraction and modeling it from the perspective of Einstein-like oscillators (Note S2, Supporting Information). This was done for the high temperature disordered phases, where all Ag^+ ions were constrained to have the same isotropic displacement parameters.

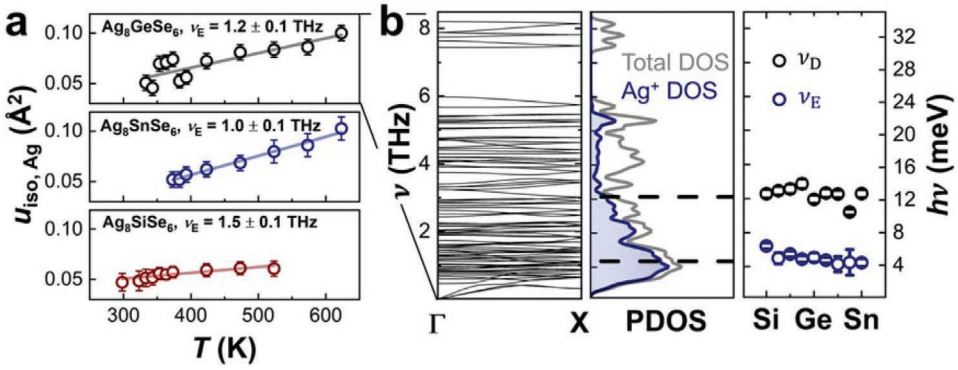

Figure 3. Structural and vibrational characterization of Ag^+ argyrodites. a) An increase in the thermal displacement parameter of Ag^+ is observed with increasing temperature, corresponding to Einstein frequencies in the range of $\nu_E = 1.0 \pm 0.1$ THz to $\nu_E = 1.5 \pm 0.1$ THz. b) A section of the phonon band structure of the orthorhombic phase of Ag_8GeSe_6 showing an avoided-crossing at low frequencies and rather dispersion-less phonon branches in agreement with the concept of Einstein-like modes (left). The phonon density of states shows that the low-frequency modes are predominantly comprised of Ag^+ vibrations (middle). Comparison of experimental Ag^+ Einstein frequencies shows good agreement with the low-frequency peak of the Ag^+-projected DOS, whereas the Debye frequencies lie near the center of the phonon DOS (right, dashed lines in DOS for reference).

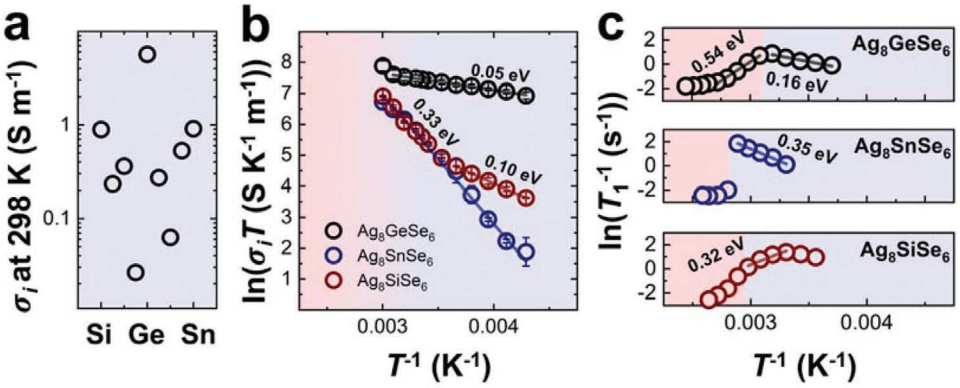

Figure 4. Ionic transport of Ag_8MSe_6. a) Room-temperature ionic conductivity as a function of the substitutional degree showing a variation of two orders of magnitude. b) Arrhenius-like temperature dependence of ionic transport, where the slope is defined by the activation barrier E_A, as obtained from impedance spectroscopy measurements of the ionic conductivity σ_i. Blue and red shading indicate the temperature range of the respective low- and high-temperature phases. c) Arrhenius plot of the ^{109}Ag T_1 relaxation times determined from nuclear magnetic resonance spectroscopy, corroborating the magnitudes of E_A found from impedance spectroscopy.

While anisotropic displacements are prevalent in ionic conductors, the partial occupation of multiple symmetry-reduced sites already describes the electron density that could otherwise be accounted for by anisotropic displacements.[55] The magnitude and temperature-dependence of the isotropic displacements match those theoretically determined from density functional theory for the low temperature phase (approximated to higher temperatures), which gives confidence that our Einstein-oscillator model describes the Ag^+ dynamics with sufficient accuracy (Note S2, Supporting Information).

The measured average Ag^+ Einstein frequency of all argyrodite compositions is 1.2 ± 0.2 THz (range = 1.0–1.5 THz, **Figure 3**a, Note S2, Supporting Information). As expected, this value is slightly lower than the average Ag^+ frequency found computationally (2.1 THz). In fact, it appears that the determined Einstein frequencies correspond to the lowest frequency peak in the vibrational density of states, with no significant change observed upon substitution (Figure 3b). The avoided-crossing features observed at ≈0.5 THz, as well as the dispersion-less nature of most optical phonon modes, justifies the use of Einstein-like frequencies to describe these low frequency Ag^+ modes (Figure 3b). Meanwhile, the average Debye frequency (3.1 ± 0.2 THz; range = 2.5–3.4 THz, Note S4, Supporting Information) found from speed of sound measurements does capture the average vibrational frequency of the entire density of states (≈3 THz), again without significant influence by substitution.

The consistency of ν_D and ν_E between all investigated argyrodites indicates that the lattice dynamical calculations and two-channel modeling of Ag_8GeSe_6 can be generalized to all compositions. This is not surprising given the minor compositional changes (≈7 at.% max.) and the fact that the largest contributions to thermal transport originate from the frequency range where Ag^+ modes are predominant (Figure 2c, Figure 3b). As mentioned earlier, the substituted species corresponds to the high frequency modes, which play an overall negligible role for thermal transport as shown by our spectral analysis (Figure 2c, Note S5, Supporting Information).

Consequently, the ultra-low thermal conductivity in these materials can be ascribed to diffuson-dominated thermal transport resulting from the energetic proximity of many vibrational modes and sufficient anharmonicity (enabling their overlap), especially in the low to mid frequency regime (Figure 2c, Figure 3b, Note S6, Supporting Information). However, it is not clear how the extent of energetic overlap of the vibrations of the mobile ion with themselves or those of the host lattice may pertain to fast ion transport.

2.3. Ag^+ Ionic Transport

A paramount contribution of this study is the concurrent characterization of thermal and ionic transport on the same materials. Here, we evaluate the magnitude and temperature dependence of the ionic conductivity of $Ag_8(Si,Ge,Sn)Se_6$ solid solutions (see Note S8, Supporting Information). All experimental data and analyses can be found in Note S8, Supporting Information. The ionic conductivities are found to vary strongly upon substitution with room-temperature values ranging from 0.088 to 5.8 S m^{-1} as determined by impedance spectroscopy (**Figure 4**a). The respective Arrhenius behavior for Ag_8SiSe_6, Ag_8GeSe_6, and Ag_8SnSe_6 reveals significant changes to the activation barrier and, with that, the temperature dependence of ionic transport (Figure 4b, all compositions: Note S8, Supporting Information). Here, Ag_8GeSe_6 exhibits the lowest activation barrier of 0.05 eV while both Ag_8SiSe_6 and Ag_8SnSe_6 show larger barriers of ≈0.3 eV at temperatures above 298 K. A change of the activation barrier at 273 K was observed for Ag_8SiSe_6 (and Si-rich compounds, Note S8, Supporting Information) suggesting a second phase transition upon cooling, which agrees with a kink observed in thermal transport measurements in the same temperature regime (Note S3, Supporting Information). The activation barriers measured by impedance spectroscopy are confirmed by ^{109}Ag nuclear magnetic resonance spectroscopy (Figure 4c), which indicates that the activation energies are predominantly a bulk property of the solid and not caused by microstructural differences. These results confirm that the Ag^+ argyrodites have significant ionic conduction, which can be changed orders of magnitude by substitution.

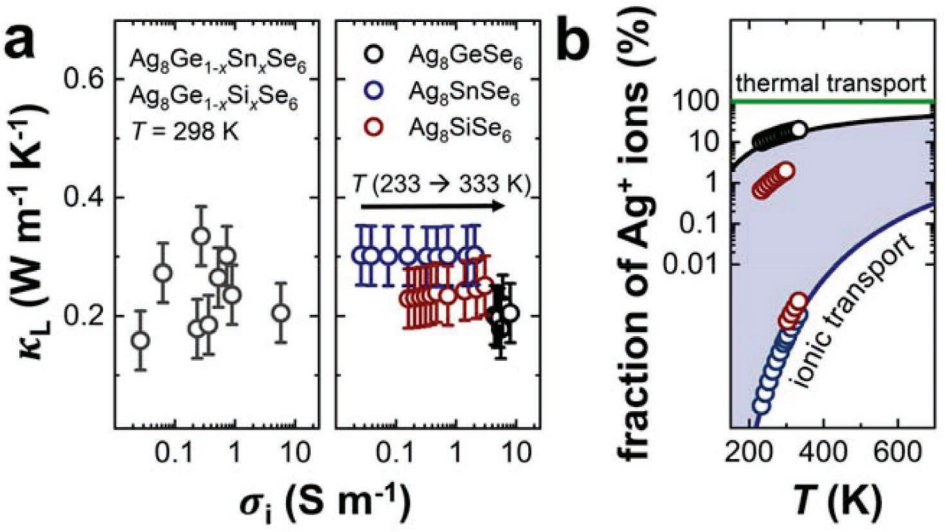

Figure 5. Direct comparison of ion and thermal conduction. a) By comparing a large number of compositions (left), it can be seen, that there is no direct correlation between the magnitude of ionic conductivity σ_i and lattice thermal conductivity κ_L at constant temperature (298 K). This lack of correlation is also evident from comparing the temperature-dependent behavior (shown for Ag_8SiSe_6, Ag_8GeSe_6 and Ag_8SnSe_6, right). b) The fraction of Ag^+ ions participating in each transport.

2.4. Comparing Thermal and Ion Transport Magnitudes

By measuring thermal conductivities, nuclear magnetic resonance and impedance spectroscopy, we have characterized thermal and ionic transport across a broad temperature range. A direct result of this investigation is that the thermal transport, as represented by the lattice thermal conductivity, is not significantly altered by orders-of-magnitude changes in ionic conductivity (**Figure 5**a). This is not only observed for varying compositions at a given temperature (300 K, Figure 5a left), but also upon investigating the temperature-dependence over a broader temperature range, as shown for the endmembers (Figure 5a right). Thus, low thermal conductivities can arise in the ordered low-temperature phases regardless of the magnitude of their ionic conduction. In other words, the scattering of propagating phonons and the presence of diffusive modes are seemingly independent of ionic transport.

The negligible role of the magnitude of ionic transport on thermal conduction may be explained as follows. The instantaneous fraction of mobile Ag^+ participating in ionic transport is given by a Boltzmann distribution,

$$\frac{N_{\text{mobile}}}{N_{\text{total}}} = \exp\left(-\frac{E_A}{k_B T}\right) \tag{2}$$

where N_{mobile} is the number density of mobile Ag^+ ions, N_{total} is the total number density of Ag^+ ions, and E_A is the macroscopic activation barrier.[23] Consequently, even with an exceptionally low activation barrier of 0.05 eV in Ag_8GeSe_6, comparable to other superionic conductors like Cu_2Se,[56] only ≈10% of the ions are thermally mobile (without an applied electric field) at any given time over the investigated temperature range (Figure 5b). For higher activation barriers, this fraction stays well below 1%. This observation sheds light on the misconception of a "liquid-like" sublattice, given that temperatures of more than 1000 K would be necessary to even reach a 50% thermally mobile sublattice. In contrast, the spectral thermal conductivity (Figure 2c) revealed that the vibrational modes of all Ag^+ ions contribute to the transport of thermal energy at temperatures relevant for ionic transport. Although more ions become mobile with increasing temperature (Equation 2, Figure 5b), the number of Ag^+ vibrational modes transferring heat remains constant. In fact, all of the Ag^+ vibrations already conduct heat at intermediate temperatures (>100 K, Figure 2b,c). Thus, the ionic conductivity increases, while the thermal conductivity remains approximately constant at higher temperatures (Figure 5a).

Considering Figure 5, it is still possible that the presence of diffusive heat transport and ionic transport may be based on the same structural traits and bonding interactions (e.g., anharmonicity), despite there being no direct correlation between the magnitudes of both processes.

Although so far, we have only considered the possible influence of ion transport on heat transported by atomic vibrations, there is also no apparent contribution to heat transport due to convection. This is to say, ionic conduction itself does not lead to an increase in thermal transport in these materials even though convection has been suggested to transport appreciable heat in fast ion conductors.[57] Our observation is unsurprising, however, considering the magnitudes of σ_i and the ionic Lorenz number derived by Rice and Roth (see Note S9, Supporting Information).[58] It should also be mentioned that the ionic conductivities reported here are measured isothermally and the Soret effect is expected to negligibly influence our characterization of the vibrational modes.

2.5. Thermal and Ionic Transport in Context of Phonon Occupations

A comparison of the ionic and thermal transport, i.e., the respective conductivities, shows that the transport processes are

seemingly independent on the macroscopic scale in the here investigated materials. Nevertheless, the direct comparison of the theoretical results provides insights into their differences on a microscopic scale: by discussing phonon occupation fluctuations. Although this is one of the standard perspectives for thermal transport analysis, this is a new viewpoint on ionics.

Thermal transport in solids arises from any deviation $(n_i - n_i^0) \neq 0$ from the equilibrium phonon occupation number n_i^0, with n_i being the instantaneous number of phonons in vibrational mode i in a given ion.[29,30] For simplicity, since we are discussing average properties, we now remove the subscript per vibrational mode; however, a full description is given in Note S10, Supporting Information. The character of the phonon mode determines the rate of thermal energy exchange (e.g., phonon-gas-like or diffuson-like).[8,15,16] In contrast to thermal transport, ionic motion can be described as an activated process such that a critical fluctuation has to be reached for the ion to overcome the activation barrier. This is a simple extension of the idea that ions receive the necessary energy for a jump from lattice vibrations, as given in the multi-excitation entropy model.[32,59] The magnitude of this critical fluctuation will depend on the vibrational mode(s) involved and the activation barrier(s) the ion faces. For a single vibrational mode, the critical number of phonons n^c required for a jump to occur is

$$n \geq n^c = \frac{\varepsilon_A}{h\nu} \tag{3}$$

where ν is the frequency of the phonon mode and ε_A corresponds to the activation barrier of this particular jump (for a mode-specific description see Supporting Information 10). Intuitively, larger barriers require larger phonon fluctuations. Considering the average Ag^+ Einstein frequency determined experimentally, where $h\nu \approx 5$ meV (1.2 THz, Figure 3b), then $n^c \approx 10$ to 100 phonons using measured macroscopic values of E_A (50 to 500 meV) for ε_A in Equation (3).

In comparison, the average phonon occupation n^0 can be calculated using the Bose–Einstein distribution function (Note S10, Supporting Information), which leads to $n^0 \approx 4.7$ phonons at 300 K for the average Ag^+ Einstein frequency ($h\nu \approx 5$ meV, 1.2 THz). This suggests that, in general, the critical fluctuation n^c is larger than the average phonon occupation n^0 of the mobile ion vibrational modes at temperatures relevant to functional ionics (e.g., solid-state batteries).

The concept of critical phonon occupation thus gives a microscopic explanation for the differences between ionic and thermal transport: thermal transport is dominated by close-to-average fluctuations of the phonon occupation while a successful ion jump requires a less likely, critical fluctuation. Because lower frequency vibrations have intrinsically higher average phonon occupations, they are expected to be more beneficial for ion transport (Note S10, Supporting Information). This is illustrated by weighting the Ag^+ partial density of states by n^0 (the Bose–Einstein distribution function) at 300 K (**Figure 6**a). A similar weighting approach was utilized by Krenzer et al. to account for the temperature-dependence of the mobile-ion band center.[9] The conclusion that lower frequency vibrations are beneficial is in agreement with the empirical observation that a softening of the lattice, i.e., lowering the vibrational frequencies, can improve the ionic conductivity.[21,60]

The average of the n^0-weighted Ag^+ density of states at 300 K is 1.2 THz. This exactly matches the aforementioned experimental average Ag^+ Einstein frequency (Figure 3), suggesting that Einstein frequencies can, in fact, be a good descriptor for the vibrations relevant for ionic transport. Upon closer inspection, this agreement is intuitive since the experimental Einstein frequencies are obtained from the vibrational motions of the mobile ions, i.e., their isotropic displacement with temperature, which are the result of only those vibrational modes that are sufficiently occupied at the measurement temperature. This has important consequences for ion conduction. First, the local ion dynamics can be tracked experimentally, and second, these need to be tailored rather than the global lattice dynamics.[19,21] The inherently low frequencies of Ag^+ vibrations in the Ag_8MSe_6 argyrodites lead to larger phonon occupations around

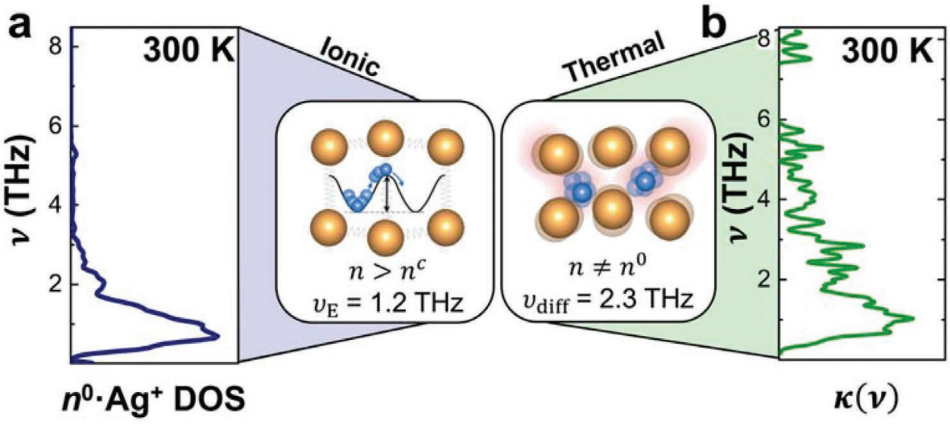

Figure 6. Relations between ionic and thermal transport. a) The Ag^+ partial density of states multiplied by the average phonon occupation $n^0(\nu)$ at 300 K with an average frequency of 1.2 THz. The criteria for ion transport, to exceed a critical phonon occupation n^c, is shown schematically. b) The corresponding spectral decomposition of diffuson-contributions to thermal transport showing a broader frequency range with an average frequency of 2.3 THz. This comparison shows that the phonons, which are believed to be the driving force for ionic transport, have diffuson character and transfer heat accordingly.

room temperature and may thus be a contributing factor to their fast ionic conduction.

While low-frequency Ag^+ vibrations are also important for thermal transport, they are not the only contributor. All vibrational modes were found to participate in thermal transport, with the spectral diffuson-contributions spanning the whole frequency range even at 300 K (Figure 6b). Here, the average diffuson frequency found from the spectral two-channel calculation (ν_{diff} = 2.3 THz) is in excellent agreement with the value estimated experimentally (ν_{diff} = 2.2 ± 0.2 THz, range 1.9 THz to 2.4 THz) using an analytical diffuson transport model (Note S4, Supporting Information).[15] Therefore, the microscopic difference between thermal and ionic transport can be summarized as follows: thermal transport pertains to phonon occupation fluctuations of any magnitude at any frequency, while ionic transport is dominated by vibrational modes with higher average occupations (at any temperature) leading to a higher probability of a critical fluctuation (Note S10, Supporting Information).

Nevertheless, while the relevant frequency range for both transport processes may be different, our theoretical analysis reveals that the main contributions reside between 1 and 3 THz where Ag^+ makes up ≈70% of the vibrational density of states. The fact that the Ag^+ vibrations have been shown to be largely diffuson-like in nature means that diffusons are foundational to understanding both thermal and ionic transport in these materials. Consequently, the vibrational character is likely important for understanding transport processes in other ionic conductors.

2.6. Phonon Occupation Interpretation of the Meyer–Neldel Behavior

So far, our discussion of ionic transport in the context of phonon occupations has pertained to its activated behavior, i.e., the migration enthalpy ($E_A \propto \Delta H_m$) that allows for a spectral analysis of ionic transport utilizing average phonon occupations (Figure 6a). With that, the microscopic difference between thermal and ionic transport becomes evident. However, the migration entropy ΔS_m is crucially important for ionic conduction as well, because it contributes exponentially to the prefactor of ionic conductivity, $\sigma_0 \propto \exp(\Delta S_m)$. The logarithm of the conductivity prefactor is commonly found to scale linearly with the activation barrier, $\ln(\sigma_0) \propto E_A$, which is also observed in this study (**Figure 7**).[32,39] This so-called Meyer–Neldel behavior is attributed to the interrelation between the migration enthalpy and entropy, i.e., $\Delta S_m \propto \Delta H_m$, and represents a bottleneck for achieving higher ionic conductivities, since lowering the activation barrier has detrimental effects on the conductivity prefactor.[21,23,32,39] Thus, understanding their interrelation is critical for the design of solid-state ionics, which are becoming increasingly relevant for the performance optimization of all solid-state batteries.[38,61]

The Meyer–Neldel rule has been derived before using the multi-excitation entropy model.[32,33] Essentially, the multi-excitation entropy model applied to ionic conductors considers that the migrational entropy arises from a multiplicity of statistical microstates associated with the absorption of phonon excitations by the mobile ions. This leads to the result that the inverse slope of the Meyer–Neldel plot (Figure 7) relates to an energy scale, corresponding to the isokinetic temperature T_{iso} ($\text{slope}^{-1} = k_B T_{iso}$),[33] and is suggested to be related to a characteristic vibrational mode, $h\nu$, as well as a characteristic number of vibrations N ($\text{slope}^{-1} = h\nu/\ln(N)$, Figure 7).[32,33] However, lacking a consistent definition of N, $\ln(N)$ is empirically treated as a coupling constant.[32,33] Thus, a deeper understanding of Meyer–Neldel behavior is still needed to develop a predictive theory based on the vibrational spectrum of the ion conductor.

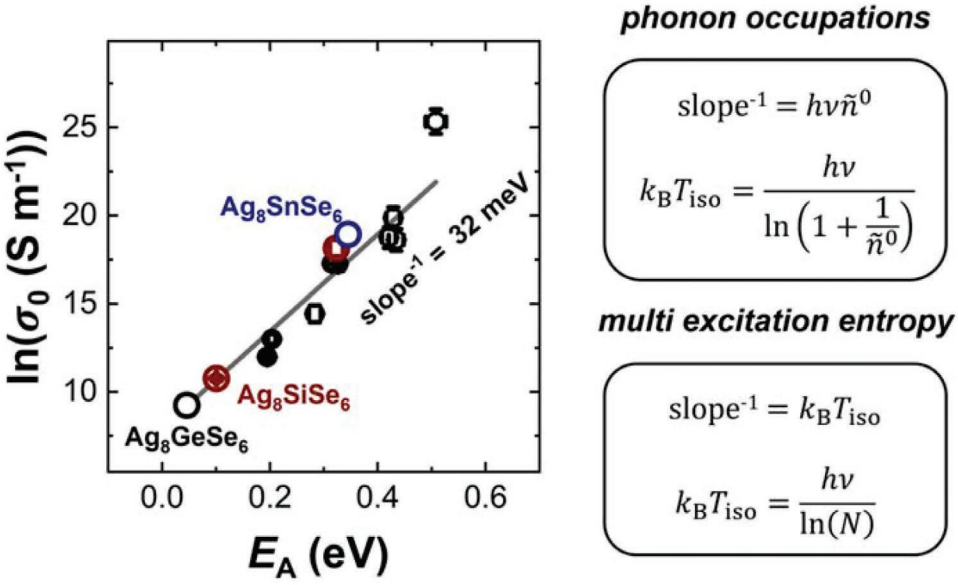

Figure 7. New interpretation of the Meyer–Neldel rule. (left) Analysis of the temperature-dependent ionic conductivities reveals an interrelation between the logarithm of the conductivity prefactor and the activation barrier, the so-called Meyer–Neldel rule, which is found to be approximately linear. (right) A derivation explaining Meyer–Neldel behavior from the viewpoint of phonon occupations provides a new interpretation of the inverse slope, and suggests that the coupling constant N from the multi excitation entropy model can now be defined.

By expounding upon the known multi-excitation entropy model[32,33] using phonon occupation fluctuation considerations, we show that the inverse Meyer–Neldel slope can be related to the vibrational modes contributing to ionic conduction and a characteristic average phonon occupation $\tilde{n}^0$ (for details see: Note S10, Supporting Information) as,[29]

$$\ln(\sigma_0) \propto \frac{\Delta S_m}{k_B} \approx \frac{E_A}{h\nu\,\tilde{n}^0} \tag{4}$$

To derive this relation, the vibrational entropy associated with fluctuations larger than the critical phonon occupation number n^c was calculated (harmonic oscillator approximation, Note S10, Supporting Information). Using the experimentally determined inverse slope (32 meV) and Ag^+ Einstein frequency at 300 K (1.2 THz, or $h\nu \approx 5$ meV), we calculate a characteristic phonon occupation $\tilde{n}^0 = 6.5$, compared to the thermal average phonon occupation of 4.7 at 300 K (again for 1.2 THz). More commonly, the Meyer–Neldel behavior is discussed in context of the full vibrational spectrum of a material.[32,39,62] Here, using the average frequency of the entire phonon density of states (3 THz) leads to a characteristic phonon occupation $\tilde{n}^0 =$ 2.6 compared to the thermal average occupation of 1.6 at 300 K. In general, Equation (4) does not make assumptions about the frequencies involved in transport, thus, it can be applied to any frequency that is assumed important for the respective material class and mobile species.

The resulting interpretation is consistent with the multi excitation entropy approach, but it leads to a physical interpretation of the coupling constant N, here related to the characteristic phonon occupation $\tilde{n}^0$.[32,33,59] This can be shown by considering that $\tilde{n}^0$ represents the average occupation of mode $h\nu$ at the isokinetic temperature T_{iso} according to the Bose–Einstein distribution function (Equation (5), Note S10, Supporting Information):

$$\tilde{n}^0 = \left(e^{\frac{h\nu}{k_B T_{iso}}} - 1\right)^{-1} \tag{5}$$

which can be algebraically solved for $k_B T_{iso}$ (Equation (6), Figure 7 right) leading to

$$k_B T_{iso} = \frac{h\nu}{\ln\left(1 + \frac{1}{\tilde{n}^0}\right)} \tag{6}$$

Comparing our results (Equation 6) to that of the multi excitation entropy model, i.e., $k_B T_{iso} = \frac{h\nu}{\ln(N)}$ (Figure 7 right), we show that the coupling constant N can be related to the characteristic phonon occupation $\tilde{n}^0$ (which is frequency-dependent following Bose–Einstein). At high isokinetic temperatures, the Bose–Einstein distribution function can be simplified to $\tilde{n}^0 \approx \frac{k_B T_{iso}}{h\nu}$, such that the inverse slope of the phonon occupation model, $h\nu\tilde{n}^0$, leads to the classical expression of $k_B T_{iso}$. Here, the relation between the coupling constant and the characteristic phonon occupation simplifies to $\ln(N) = \frac{1}{\tilde{n}^0}$. Because of the relation given by Equation (5), it is reasonable to call $\tilde{n}^0$ the isokinetic phonon occupation.

Understanding phonon occupations in ionic conductors may thus provide the key to unlocking next-generation design strategies in functional ionic materials. Given the good agreement of the phonon occupation model with the established results of the multi-exication entropy model, the evaluation of a multitude of different material classes, mobile ions and average frequencies is expected to lead to new insights and design principles for fast ionic conductors. A consequence for solid-electrolyte research would be the importance of manipulating phonon occupations (e.g., targeted phonon excitation,[52] through opto-electronic stimulation[63]) in conjunction with tailoring the atom-specific vibrational frequencies and local activation energies.

3. Conclusion

This work demonstrates that diffuson-mediated thermal transport is dominant in Ag^+ argyrodite fast ionic conductors at temperatures relevant for thermoelectrics and ionic transport. An important consequence of this fact is that ionic conductivity can be varied by orders of magnitude without affecting the thermal conductivity, which has drastic implications for thermoelectric materials and device design. The similarities of the argyrodite structure with lithium and sodium superionic conductors mean that diffusons are likely prevalent in battery materials as well. In general, a vibrational perspective of ionic transport can be greatly aided by thermal transport analysis. Here, new insights into Meyer–Neldel behavior have been shown to relate phonon occupations with the typically used isokinetic temperatures. Thus, by understanding the origins of thermal and ionic transport, in particular via vibrational characteristics and phonon occupations, novel design concepts are possible to further improve functional ionic conducting materials.

Supporting Information

Supporting Information is available from the Wiley Online Library or from the author.

Acknowledgements

The research was supported by the Deutsche Forschungsgemeinschaft (DFG) under grant number ZE 1010/5-1. B.W. is a member of the International Graduate School for Battery Chemistry, Characterization, Analysis, Recycling and Application (BACCARA), which is funded by the Ministry for Culture and Science of North Rhine Westphalia, Germany. M.T.A. acknowledges the Alexander von Humboldt Foundation for financial support through a Postdoctoral Fellowship. The authors acknowledge access to various computational resources: The Tier-1 supercomputer of the Fédération Wallonie-Bruxelles funded by the Walloon Region (grant agreement no. 1117545), and all the facilities provided by the Université catholique de Louvain (CISM/UCL) and by the Consortium des Equipements de Calcul Intensif en Fédération Wallonie-Bruxelles (CECI).

Open access funding enabled and organized by Projekt DEAL.

Conflict of Interest

The authors declare no conflict of interest.

Data Availability Statement

The data that support the findings of this study are available from the corresponding author upon reasonable request.

Keywords

argyrodites, diffusons, ion conduction, Meyer–Neldel, phonon occupations, thermal transport

Received: March 1, 2022
Revised: March 31, 2022
Published online:

[1] H. Liu, X. Shi, F. Xu, L. Zhang, W. Zhang, L. Chen, Q. Li, C. Uher, T. Day, G. J. Snyder, *Nat. Mater.* **2012**, *11*, 422.
[2] B. Li, H. Wang, Y. Kawakita, Q. Zhang, M. Feygenson, H. L. Yu, D. Wu, K. Ohara, T. Kikuchi, K. Shibata, T. Yamada, X. K. Ning, Y. Chen, J. Q. He, D. Vaknin, R. Q. Wu, K. Nakajima, M. G. Kanatzidis, *Nat. Mater.* **2018**, *17*, 226.
[3] B. Jiang, P. Qiu, H. Chen, Q. Zhang, K. Zhao, D. Ren, X. Shi, L. Chen, *Chem. Commun.* **2017**, *53*, 11658.
[4] J. Ding, J. L. Niedziela, D. Bansal, J. Wang, X. He, A. F. May, G. Ehlers, D. L. Abernathy, A. Said, A. Alatas, Y. Ren, G. Arya, O. Delaire, *Proc. Natl. Acad. Sci. USA* **2020**, *117*, 3930.
[5] J. L. Niedziela, D. Bansal, A. F. May, J. Ding, T. Lanigan-Atkins, G. Ehlers, D. L. Abernathy, A. Said, O. Delaire, *Nat. Phys.* **2019**, *15*, 73.
[6] S. Schwarzmüller, M. Jakob, M. Nentwig, T. Schröder, A. Kuhn, A. Düvel, P. Heitjans, O. Oeckler, *Chem. Mater.* **2018**, *30*, 7970.
[7] E. S. Toberer, A. Zevalkink, G. J. Snyder, *J. Mater. Chem.* **2011**, *21*, 15843.
[8] R. Hanus, R. Gurunathan, L. Lindsay, M. T. Agne, J. Shi, S. Graham, G. J. Snyder, *Appl. Phys. Rev.* **2021**, *8*, 031311.
[9] G. Krenzer, C.-E. Kim, K. Tolborg, B. J. Morgan, A. Walsh, *J. Mater. Chem. A* **2021**, *10*, 2295.
[10] S. Lin, W. Li, S. Li, X. Zhang, Z. Chen, Y. Xu, Y. Chen, Y. Pei, *Joule* **2017**, *1*, 816.
[11] S. Lin, W. Li, Y. Pei, *Mater. Today* **2021**, *48*, 40.
[12] R. Hanus, M. T. Agne, A. J. E. Rettie, Z. Chen, G. Tan, D. Y. Chung, M. G. Kanatzidis, Y. Pei, P. W. Voorhees, G. J. Snyder, *Adv. Mater.* **2019**, *31*, 1900108.
[13] P. B. Allen, J. L. Feldman, J. Fabian, F. Wooten, *Philos. Mag. B* **1999**, *79*, 1715.
[14] P. B. Allen, J. L. Feldman, *Phys. Rev. B* **1993**, *48*, 12581.
[15] M. T. Agne, R. Hanus, G. J. Snyder, *Energy Environ. Sci.* **2018**, *11*, 609.
[16] R. Hanus, J. George, M. Wood, A. Bonkowski, Y. Cheng, D. L. Abernathy, M. E. Manley, G. Hautier, G. J. Snyder, R. P. Herrmann, *Mater. Today Phys.* **2021**, *18*, 100344.
[17] M. Simoncelli, N. Marzari, F. Mauri, *Nat. Phys.* **2019**, *15*, 809.
[18] P. B. Allen, J. L. Feldman, *Phys. Rev. Lett.* **1989**, *63*, 645.
[19] T. Krauskopf, S. Muy, S. P. Culver, S. Ohno, O. Delaire, Y. Shao-Horn, W. G. Zeier, *J. Am. Chem. Soc.* **2018**, *140*, 14464.
[20] Z. Cheng, B. Zahiri, X. Ji, C. Chen, D. Chalise, P. V. Braun, D. G. Cahill, *Small* **2021**, *17*, 2101693.
[21] M. A. Kraft, S. P. Culver, M. Calderon, F. Böcher, T. Krauskopf, A. Senyshyn, C. Dietrich, A. Zevalkink, J. Janek, W. G. Zeier, *J. Am. Chem. Soc.* **2017**, *139*, 10909.
[22] J. B. Boyce, B. A. Huberman, *Phys. Rep.* **1979**, *51*, 189.
[23] S. Ohno, A. Banik, G. F. Dewald, M. A. Kraft, T. Krauskopf, N. Minafra, P. Till, M. Weiss, W. G. Zeier, *Prog. Energy* **2020**, *2*, 022001.
[24] S. P. Culver, T. Krauskopf, R. Koerver, W. G. Zeier, *Chem. Mater.* **2018**, *30*, 4179.
[25] W. Li, S. Lin, B. Ge, J. Yang, W. Zhang, Y. Pei, *Adv. Sci.* **2016**, *3*, 1600196.
[26] F. Reissig, B. Heep, M. Panthöfer, M. Wood, S. Anand, G. J. Snyder, W. Tremel, *Dalton Trans.* **2019**, *48*, 15822.
[27] N. M. Vargas-Barbosa, B. Roling, *ChemElectroChem* **2020**, *7*, 367.
[28] P. Bruesch, L. Pietronero, S. Strassler, H. R. Zeller, *Phys. Rev. B* **1977**, *15*, 4631.
[29] J. M. Ziman, *Electrons and Phonons. The Theory of Transport Phenomena in Solids*, Oxford University Press, London **1963**.
[30] HardyR. J. , *Phys. Rev.* **1963**, *132*, 168.
[31] H. R. Seyf, W. Lv, A. Rohskopf, A. Henry, *Sci. Rep.* **2018**, *8*, 2627.
[32] A. Yelon, B. Movaghar, R. S. Crandall, *Rep. Prog. Phys.* **2006**, *69*, 1145.
[33] P. Du, N. Li, X. Ling, Z. Fan, A. Braun, W. Yang, Q. Chen, A. Yelon, *Adv. Energy Mater.* **2021**, *12*, 2102939.
[34] S. Acharya, J. Pandey, A. Soni, *ACS Appl. Energy Mater.* **2019**, *2*, 654.
[35] B. K. Heep, K. S. Weldert, Y. Krysiak, T. W. Day, W. G. Zeier, U. Kolb, G. J. Snyder, W. Tremel, *Chem. Mater.* **2017**, *29*, 4833.
[36] Q. Jiang, S. Li, Y. Luo, J. Xin, S. Li, W. Li, G. Zhao, J. Yang, *ACS Appl. Mater. Interfaces* **2020**, *12*, 54653.
[37] P. Qiu, M. T. Agne, Y. Liu, Y. Zhu, H. Chen, T. Mao, J. Yang, W. Zhang, S. M. Haile, W. G. Zeier, J. Janek, C. Uher, X. Shi, L. Chen, G. J. Snyder, *Nat. Commun.* **2018**, *9*, 4.
[38] J. Janek, W. G. Zeier, *Nat. Energy* **2016**, *1*, 16141.
[39] S. Muy, R. Schlem, Y. Shao-Horn, W. G. Zeier, *Adv. Energy Mater.* **2020**, *11*, 2002787.
[40] R. D. Shannon, *Acta Crystallogr., Sect. A: Found. Crystallogr.* **1976**, *32*, 751.
[41] Z. Jin, Y. Xiong, K. Zhao, H. Dong, Q. Ren, H. Huang, X. Qiu, J. Xiao, P. Qiu, L. Chen, X. Shi, *Mater. Today Phys.* **2021**, *19*, 100410.
[42] X. Shen, C. C. Yang, Y. Liu, G. Wang, H. Tan, Y. H. Tung, G. Wang, X. Lu, J. He, X. Zhou, *ACS Appl. Mater. Interfaces* **2019**, *11*, 2168.
[43] D. G. Cahill, S. K. Watson, R. O. Pohl, *Phys. Rev. B* **1992**, *46*, 6131.
[44] C. Yang, Y. Luo, X. Li, J. Cui, *RSC Adv.* **2021**, *11*, 3732.
[45] L. Li, Y. Liu, J. Dai, A. Hong, M. Zeng, Z. Yan, J. Xu, D. Zhang, D. Shan, S. Liu, Z. Ren, J. M. Liu, *J. Mater. Chem. C* **2016**, *4*, 5806.
[46] X. Zhang, C. L. Zhang, S. Lin, H. Lu, Y. Pei, S. Jia, *J. Appl. Phys.* **2016**, *119*, 6.
[47] G. Tan, S. Hao, R. C. Hanus, X. Zhang, S. Anand, T. P. Bailey, A. J. E. Rettie, X. Su, C. Uher, V. P. Dravid, G. J. Snyder, C. Wolverton, M. G. Kanatzidis, *ACS Energy Lett.* **2018**, *3*, 705.
[48] M. Jin, S. Lin, W. Li, Z. Chen, R. Li, X. Wang, Y. Chen, Y. Pei, *Chem. Mater.* **2019**, *31*, 2603.
[49] M. T. Agne, S. Anand, G. J. Snyder, *Research* **2022**, https://doi.org/10.34133/2022/9786705.
[50] T. M. Brenner, C. Gehrmann, R. Korobko, T. Livneh, D. A. Egger, O. Yaffe, *Phys. Rev. Mater.* **2020**, *4*, 115402.
[51] H. R. Seyf, A. Henry, *J. Appl. Phys.* **2016**, *120*, 025101.
[52] K. Gordiz, S. Muy, W. G. Zeier, Y. Shao-Horn, A. Henry, *Cell Rep. Phys. Sci.* **2021**, *2*, 100431.
[53] B. C. Sales, D. G. Mandrus, B. C. Chakoumakos, *Semicond. Semimetals* **2001**, *70*, 1.
[54] R. Hanus, X. Guo, Y. Tang, G. Li, G. J. Snyder, W. G. Zeier, *Chem. Mater.* **2017**, *29*, 1156.
[55] E. J. Cussen, *J. Mater. Chem.* **2010**, *20*, 5167.

[56] T. Takahashi, O. Yamamoto, F. Matsuyama, Y. Noda, *J. Solid State Chem.* **1976**, *16*, 35.
[57] Y. Zhou, S. Xiong, X. Zhang, S. Volz, M. Hu, *Nat. Commun.* **2018**, *9*, 4712.
[58] M. J. Rice, W. L. Roth, *J. Solid State Chem.* **1972**, *4*, 294.
[59] A. Yelon, B. Movaghar, *Phys. Rev. Lett.* **1990**, *65*, 618.
[60] T. Krauskopf, C. Pompe, M. A. Kraft, W. G. Zeier, *Chem. Mater.* **2017**, *29*, 8859.
[61] S. Ohno, T. Bernges, J. Buchheim, M. Duchardt, A. K. Hatz, M. A. Kraft, H. Kwak, A. L. Santhosha, Z. Liu, N. Minafra, F. Tsuji, A. Sakuda, R. Schlem, S. Xiong, Z. Zhang, P. Adelhelm, H. Chen, A. Hayashi, Y. S. Jung, B. V. Lotsch, B. Roling, N. M. Vargas-Barbosa, W. G. Zeier, *ACS Energy Lett.* **2020**, *5*, 910.
[62] J. Zahnow, T. Bernges, A. Wagner, N. Bohn, J. R. Binder, W. G. Zeier, M. T. Elm, J. Janek, *ACS Appl. Energy Mater.* **2021**, *4*, 1335.
[63] A. Krishnamoorthy, M. F. Lin, X. Zhang, C. Weninger, R. Ma, A. Britz, C. S. Tiwary, V. Kochat, A. Apte, J. Yang, S. Park, R. Li, X. Shen, X. Wang, R. Kalia, A. Nakano, F. Shimojo, D. Fritz, U. Bergmann, P. Ajayan, P. Vashishta, *Nano Lett.* **2019**, *19*, 4981.